Journal of Inorganic Biochemistry 239 (2023) 112068

Contents lists available at ScienceDirect

Journal of Inorganic Biochemistry

journal homepage: www.elsevier.com/locate/jinorgbio

How Cu(II) binding affects structure and dynamics of α-synuclein revealed by molecular dynamics simulations

Loizos Savva, James A. Platts *

School of Chemistry, Cardiff University, Park Place, Cardiff CF10 3AT, UK.

ARTICLE INFO

Keywords:
Parkinson's disease
Synuclein
Copper
Molecular dynamics
Metal ion
Implicit solvent

ABSTRACT

We report accelerated molecular dynamics simulations of α-Synuclein and its complex with two Cu(II) ions bound to experimentally determined binding sites. Adding two Cu(II) ions, one bound to the N-terminal region and one to the C-terminus, decreases size and flexibility of the peptide while introducing significant new contacts within and between N-terminus and non-Aβ component (NAC). Cu(II) ions also alter the pattern of secondary structure within the peptide, inducing more and longer-lasting elements of secondary structure such as β-strands and hairpins. Free energy surfaces, obtained from reweighting the accelerated molecular dynamics boost potential, further demonstrate the restriction on size and flexibility that results from binding of copper ions.

1. Introduction

α-Synuclein (αS) is a 140-residue protein that has been associated with Parkinson's disease (PD), where it has been found to accumulate in Lewy bodies and other pathological aggregates [1]. Aggregation of αS has also been reported in Alzheimer's disease (AD), through the central hydrophobic non-amyloid-β component (NAC), residues 61–95, Fig. 1 [2]. The spatiotemporal heterogeneity of intrinsically disordered proteins (IDPs) such as αS has been reported to be influenced by environmental factors, with function-related conformations with varied retention times, depending on the peptide and interactions with binding partners [3,4]. Promotion of fibrillation of αS has been proposed as a result of various environmental factors, such as low pH and increased temperature, owing to a decrease in the diffusivity of the aggregates [5,6].

Transition metal ions [7–11], which have inspired this study, have been observed to affect fibril formation. αS has been suggested to aggregate intracellularly as a response to divalent metal ions (Fe(II), Mn (II), Co(II), Ni(II) and in particular Cu(II)), bound to the two termini, with the removal of either coordinated metal resulting in disruption of aggregation [12,13]. Some reports have been published on the role of metal ions in the promotion of free-radical mediated oxidative processes [14–16], with most focusing either on the specific regions interacting with the ions [8,10,11,17–24], or the possible self-oligomerisation and aggregation mechanisms involving the metal ions [9,12,25,26]. Studies employing small-angle X-ray scattering (SAXS), nuclear magnetic resonance (NMR), circular dichroism (CD) and electron paramagnetic resonance (EPR) spectroscopy, on metal ion-αS interactions, implicate regions M_1DVFMKGLS$_9$, V_{48}AHGV$_{52}$ and D_{119}PDNEA$_{124}$ as the metal ion-binding sites [8,10,20,27]. Further research into the specific binding modes of these metal ions and the aforementioned sites, proposed one of those to consist of macro-chelation between residues M1, D2 and H50, and a second site encompassing D119, D121, N122 and E123 [8,11]. We note that Cu(II)-coordination at the N-terminus has also been proposed to occur through either coordination with M1, D2 and H_2O, or V49, H50 and H_2O [28,29]. The former has also been thought to exist in the membrane-bound form of αS, while the latter has been linked to the acetylated form of αS [30,31]. In its monomeric WT form, however, these binding modes have been put into dispute from electron spin-echo envelope modulation (ESEEM) spectroscopy studies [32–34], thus here we focus only on the more established macro-chelated coordination mode [20,32–36]. This coordination mode has also been proposed to happen in an interpeptide fashion, although that aspect has not been explored herein [37]. The coordination of the first site occurs in a 3N1O fashion, while the C-terminal binding involves a 4O coordination mode [8,11,18,38]. These binding modes are presented in Fig. 2. One of the anchoring residues for metal ions, especially Cu(II), binding on the peptide chain is H50. In this context, it is notable that a H50A mutant results in quite different aggregation profile on coordination with Cu(II) compared to the wild type [12,20,39].

Computational studies on the binding of Cu(II) to αS are less prominent in literature compared to experiment, with most of the published

* Corresponding author.
E-mail address: platts@cardiff.ac.uk (J.A. Platts).

https://doi.org/10.1016/j.jinorgbio.2022.112068
Received 20 September 2022; Received in revised form 8 November 2022; Accepted 8 November 2022
Available online 13 November 2022

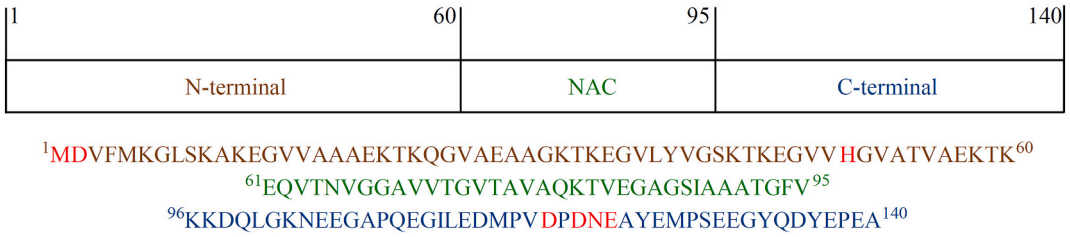

Fig. 1. Primary structure of αS. The sites involved in metal ion binding include: M1, D2, H50, D119, D121, N122, E123 are highlighted in red. (For interpretation of the references to colour in this figure legend, the reader is referred to the web version of this article.)

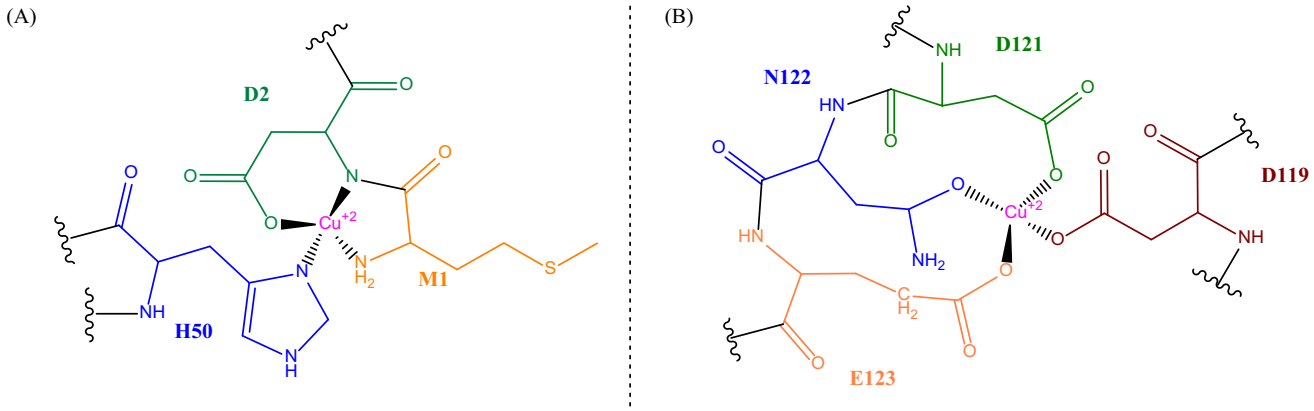

Fig. 2. Schematic of the two metal ion binding sites, in a (A) 3N1O fashion at the N- and (B) 4O at the C-termini.

Table 1
Force constants and equilibrium distances of coordinating atoms to metal centres, as calculated from B3LYP/6-31G(d) optimisation of the metal sites.

Metal site	Ligating atoms	Force constant (kCal/mol·Å^{-2})	Equilibrium distance (Å)
N-terminal	MET1 (N)	110.6	1.910
	ASP2 (N)	128.6	1.881
	ASP2 (O)	90.70	1.929
	HIS50 (N)	127.0	1.913
C-terminal	ASP119 (O)	93.20	1.905
	ASP121 (O)	117.8	1.879
	ASN122 (O)	1.400	2.298
	GLU123 (O)	54.20	2.030

Table 2
Literature survey of reported secondary structural characteristics from different experimental methods.

Method	Reference	Conditions	α-helix (%)	β-strand (%)	Other (%)
Circular Dichroism	[78]	Untreated αS (0.074 mg/mL), 293.15 K, pH 7.4	2 ± 3	11 ± 7	86 ± 22
	[79]	αS (0.2 mg/mL), Tris-HCl (25 mM), NaCl (50 mM), 293.15 K, pH 7.4	~0	31	68
	[80]	purified αS from mouse brain (7.5 μM), PBS[a] (25%), 293.15 K, pH 7.4	22.5 ± 1.5	n/a	46.5 ± 12.5
	[81]	αS (2.0 mg/mL), PBS[a] (100 mM), NaCl (100 mM), pH 7.4	19 ± 1	n/a	n/a
Raman Spectroscopy	[82]	αS (200 μM), Tris-HCl (20 mM), pH 7.5	49	10	41
	[83]	αS (300 μM), PBS[a] (20 mM), pH 7.5	48	15	37
ATR-FTIR Spectroscopy	[77]	Supernatant αS {from lyophilized sample (2–5 mg) dissolved in ddH_2O, NaOH (100 mM), pH 10 ± 0.5, incubated at 293.15 K and centrifuged for 30 min}, HCl (1 mM), Tris-HCl, pH 7.4	35	3	62

[a] Phosphate-buffered saline.

ones focusing on modelling the free peptide [17,18,36,40]. One of the challenges to be addressed is the parameterisation of the metal ion. A well-established method to approach this issue is the use of density functional theory (DFT), which properly accounts for the electronic effects of the metal ion. However, the flexibility of IDPs and requirement for sampling the many conformations accessible to αS under biological conditions, mean that the computational overhead of DFT, or even hybrid QM/MM, becomes prohibitive. A more tractable approach is to extract molecular mechanics (MM) force field parameters from DFT calculations [41], and then to use these to perform molecular dynamics (MD) simulations. The intrinsically disordered nature of the peptide has to be taken into consideration when choosing the force field [40,42,43]. Here, we employ ff03ws [42] with the Onufriev, Bashford, Case (OBC) implicit solvent model, having performed an evaluation of the combination in a previous study involving metal-free α-Synuclein [44], showing that it reproduces experimental values of size, secondary

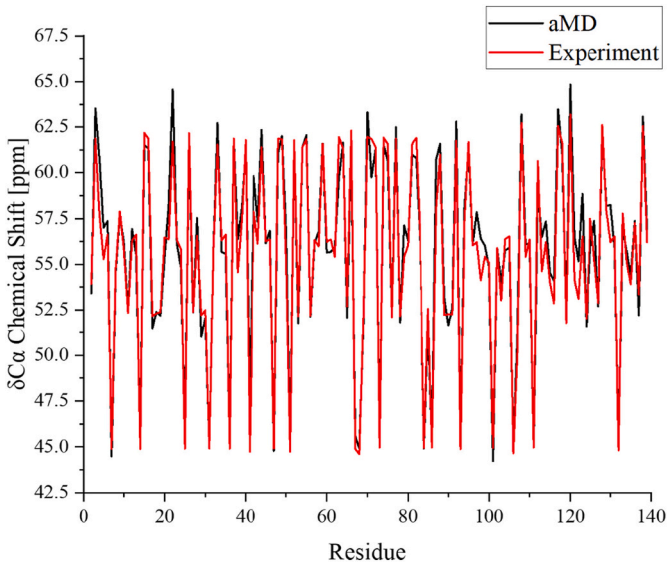

Fig. 3. Predicted Cα chemical shift values per residue, from 1200 frames taken from the accelerated MD simulations on αS (black). Experimental data (red) obtained from source [84]. (For interpretation of the references to colour in this figure legend, the reader is referred to the web version of this article.)

structure and backbone chemical shift. The choice of implicit solvent also addressed the generally low radius of gyration (R_g) values reported both in our prior computational study, but also throughout the literature, where explicit solvents are used, reporting around 10 Å lower expansion [45] compared to experimental findings [5,46]. A recent study [47], analysed the MD data amounting to 73 μs produced by the D. E. Shaw Research (DESRES) group [48], extracting the major conformational components they compared these to experimental results from single-molecule force spectroscopy [49,50], single-molecule Förster resonance energy transfer [51] and other experimental and computational results, concluding the experimental classification of random coil interactions was the most populated, while the corresponding clusters from the MD simulations, appeared to underestimate the random coil and overestimate the strong-interacting experimental populations. The MD simulations by DESRES were performed in explicit solvent, maintaining the overestimation of the more restricted conformation of αS, when simulated using explicit models [52,53].

Two QM/MM studies examined the coordination of Cu(II) in the N-terminus of αS, one of them looking at the M1-D2-H_2O binding site [54], believed to result in the more stable Cu(II)-complex, owing to the formation of a (5,6)-joined chelate ring from (NH2, N^-, β-COO^-) [55]; while the other focusing on the V48-H50 region [39], involved in the Cu(II)-coordination of the N-terminally acetylated αS [56]. One of the computational studies employing MD simulations to study the copper-bound peptide involved a fragment of αS, simulating the first 12 residues, coordinating the copper ion on the first two amino acids and a water molecule. The temperature replica-exchange molecular dynamics (T-REMD) simulations performed in that study, employed the ff03, CHARMM27, OPLS-AA and GROMOS43A1 force fields in explicit solvent [24]. Other computational studies on the full peptide have used coarse-grained molecular dynamics (CG-MD), through scaling seen in the ff03ws force field applied in SIRAH [17,23], and *ab initio* [18,22] and MD simulations using the CHARMM27 in explicit solvent [18]. These studies have highlighted the high affinity of Cu(II) coordination to Asp121 and His50, a feature we have also seen through the *ab initio* calculation of force constants (*vide infra*). Results on the secondary structure and R_g from those simulations, present a decrease in the helical characteristics upon copper binding with a corresponding increase in random coil, while also noting small changes in R_g distributions between unbound and copper-bound peptide.

2. Computational methods

Molecular dynamics simulations were performed using the AMBER16 package [57]. The two metal sites, where Cu(II) interacts with the peptide, were parameterised using the metal centre parameter builder (MCPB.py) program [41], using angle, bond and charge parameters obtained through Gaussian09 [58] using B3LYP/6-31G(d) [59]. The Seminario [60] method and restrained electrostatic potential (RESP) fitting scheme [61–63], were utilised to obtain harmonic force constants and atomic charges from DFT calculations. The LEaP [64] function was then used to combine these with the force field parameters. The systems were solvated with the Onufriev, Bashford, Case (OBC) modification to the generalised Born (GB) model [65–67]. The selection for the implicit solvent was made after considering the underestimation of the effective radii, which may come as a result of using macromolecules, owing to the treatment of vacuum-filled crevices as

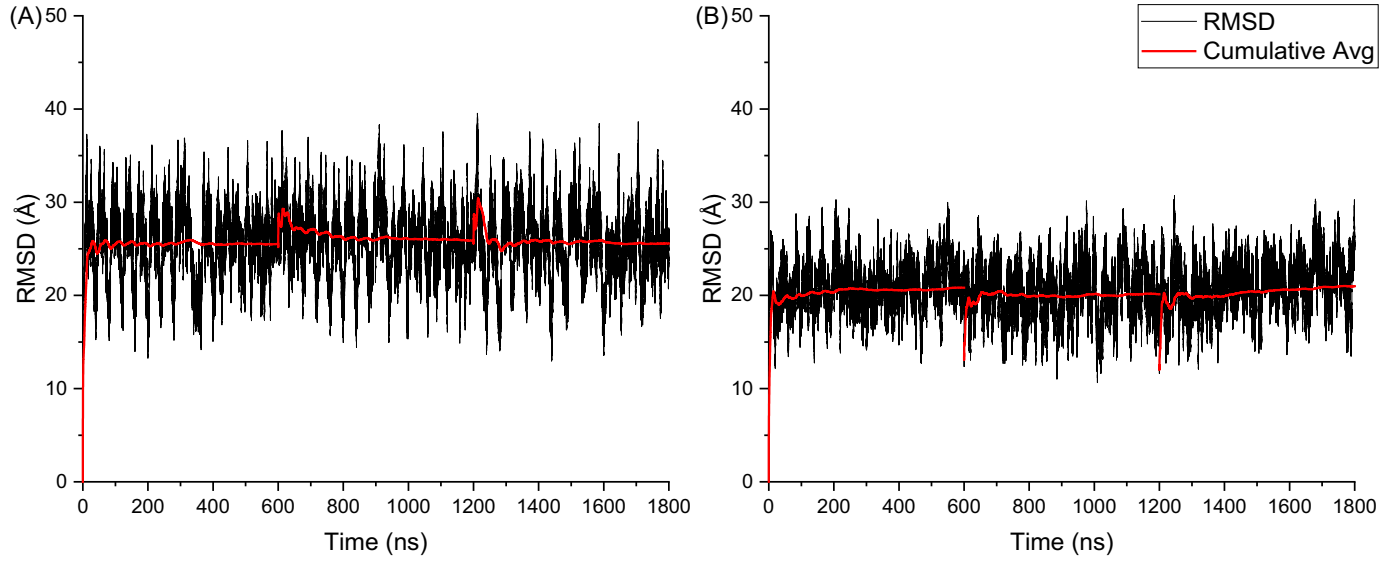

Fig. 4. RMSD relative to the cMD end-point over accelerated MD simulations, on the (A) free and (B) Cu(II)-αS, with the cumulative average shown in red. (For interpretation of the references to colour in this figure legend, the reader is referred to the web version of this article.)

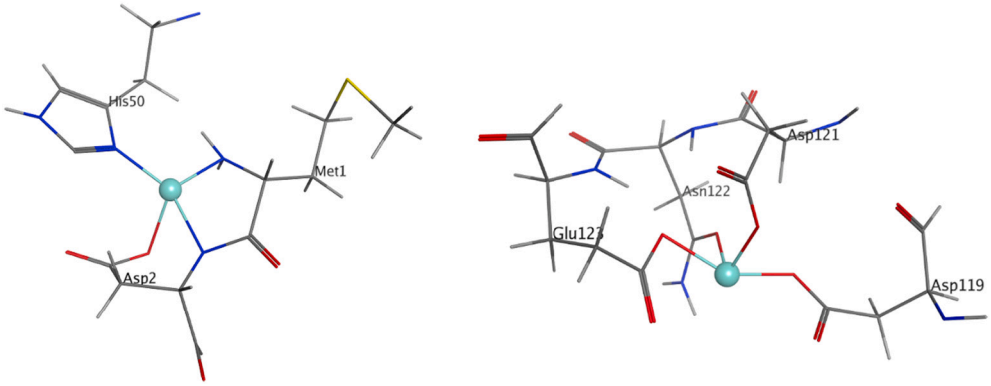

Fig. 5. Coordination of ligating atoms in each of the metal sites, from the mean cluster structure.

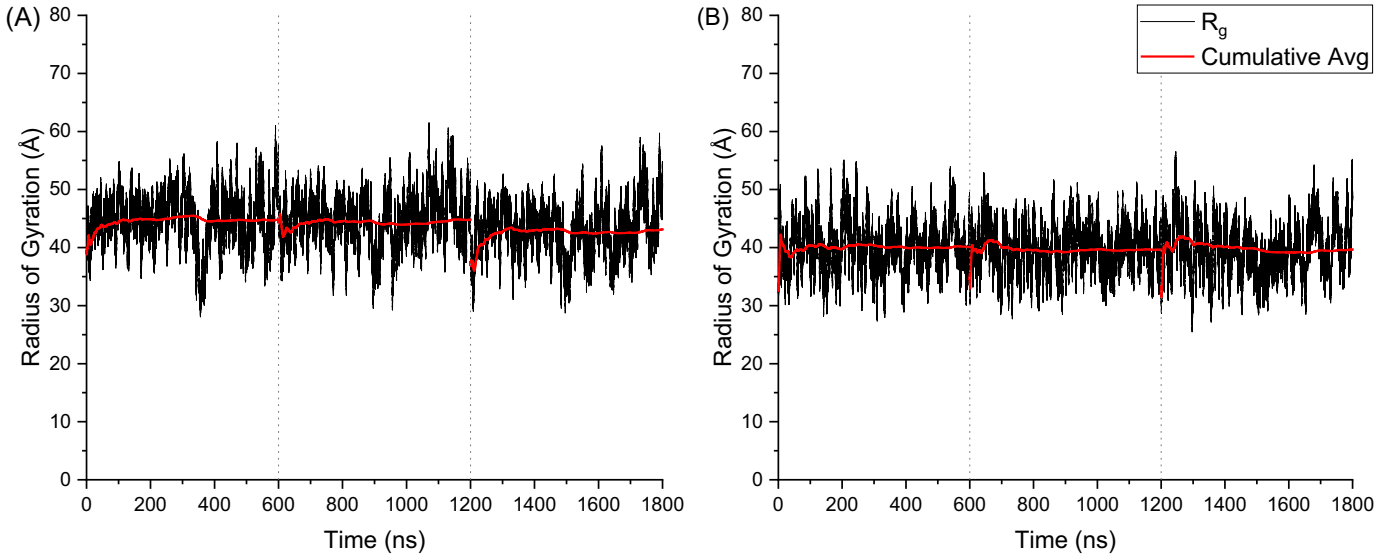

Fig. 6. Radius of gyration from aMD simulations on (A) free and (B) copper-bound peptide, with the cumulative average shown in red. (For interpretation of the references to colour in this figure legend, the reader is referred to the web version of this article.)

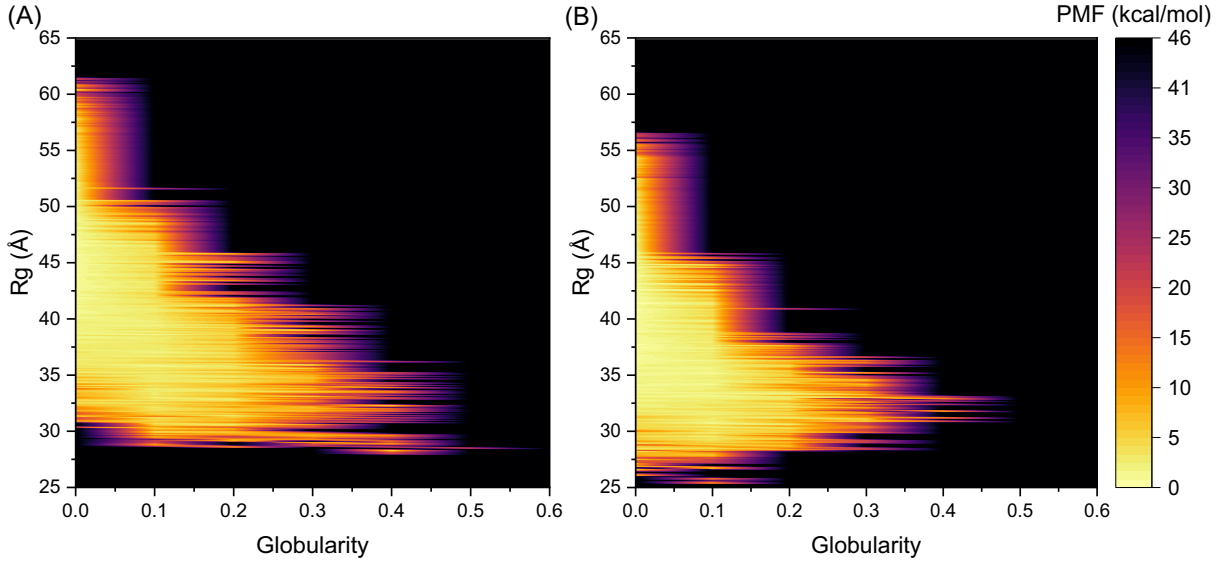

Fig. 7. 2D free energy plot of the radius of gyration (R_g) against globularity, from the aMD simulations on the (A) free and (B) copper-bound peptide.

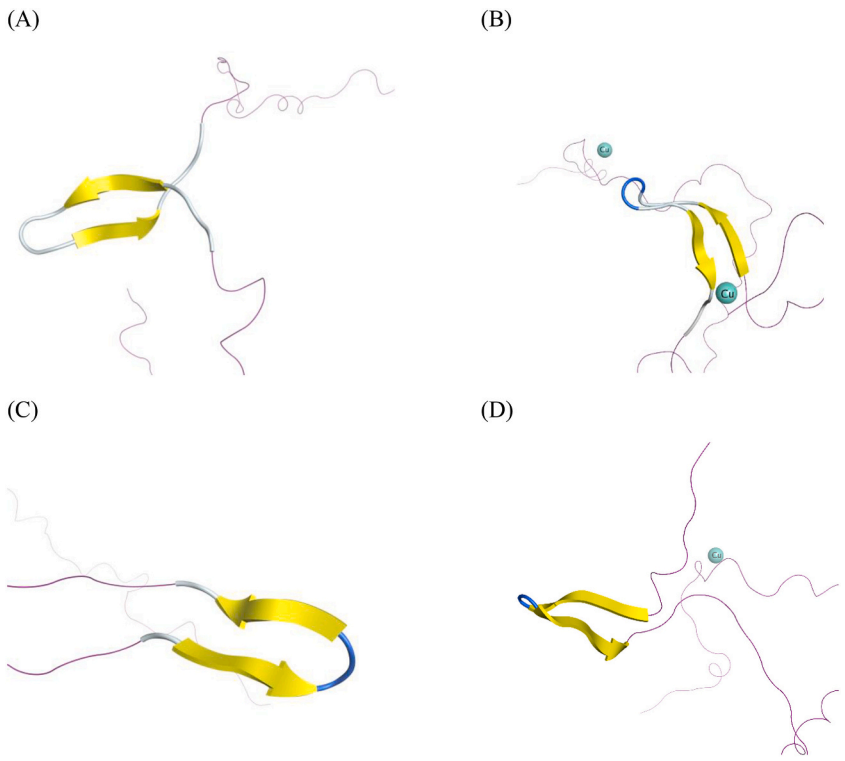

Fig. 8. β-hairpin structure (yellow) found between residues 38–53 in the (A) unbound and (B) Cu(II)-bound αS and respectively (C–D) between residues 63–72.

Table 3
R_g data for free and copper-bound peptides (Å).

	Mean R_g	SD	Max	Min
free-αS (Experimental)	40 ± 1[5] 35.5 ± 0.5[46]			
free-αS	44.26	4.58	61.50	28.07
Cu(II)-αS	39.81	4.31	56.53	25.48

Table 4
Maximum time β-hairpins are expressed in the two residue ranges of 38–53 and 63–72.

	Maximum time (ns)	
	Residues 38–53	Residues 63–72
Free-αS	42	54
Cu(II)-αS	72	60

being filled with water, especially where 'buried' atoms, in the central region of the peptide, are concerned [67]. The ff03ws force field was used here, after our group previously assessed its performance on the unbound α-Synuclein. The use of implicit solvent with this force field was also evaluated in the same study, where explicit solvent simulations appeared to not adequately match experimental findings, especially for radius of gyration, secondary structure and electrostatic interactions [17,18,36,40,44,68]. Key observations made therein on the folding characteristics are also discussed here with regards to experimental evidence on the metal-free system.

The systems studied here were modelled in their extended conformation in MOE, where they were also minimised through the ligand-field molecular mechanics (LFMM) force field embedded within DommiMOE [69]. Having minimised the two systems, three individual conventional molecular dynamics (cMD) simulations were performed each for 300 million steps at a 2 fs timestep. The MD simulations were performed in the NVT ensemble 310 K, using the Langevin thermostat [70]. The SHAKE algorithm [71] was used to impose holonomic restraints on bonds to hydrogen, restricting them to their equilibrium length. The cMD simulations are not reported here, since we previously established the superiority of the simulations performed using accelerated MD (aMD) in this system [72]. The boost potential was calculated from the mean total potential energy, imposing a bias in the simulations, pushing the peptides out of local minima in which they may get stuck in cMD simulations. Three individual aMD simulations were performed for 600 ns each, starting from the final conformation and velocity from each of the cMD trajectories. The parameters of the simulations were otherwise kept identical to the cMD simulations. Free energy landscape plots were constructed through reweighting [72], and the carma package [73] was used to obtain clusters from principal component analysis (PCA) of the cartesian coordinates of Cα, and the FindGeo [74] tool was used to assess possible geometries around the metal centres. The rest of the analysis performed using the cpptraj [75] tool, acquiring data on secondary structure, root mean square fluctuation (RMSF), salt bridges, hydrogen bonding, RMSD and radius of gyration (R_g), without reweighting of the trajectories.

3. Results and discussion

3.1. Parameterisation of metal sites

The metal sites of the modelled peptide were parameterised using the MCPB.py tool [41], after establishing the metal ion binding sites from literature survey of experimental *in vitro* and *in silico* studies on the coordination of Cu(II) [8,10,11,22,76]. DFT calculations were then performed to assign harmonic bonds between the metal ions and the atoms involved in their coordination.

Looking at the values from the QM calculations, Table 1 and Table S1, a relatively consistent force is imposed on the ligating atoms in the N-terminus. This is not the case, however, in the C-terminal metal site, where smaller force constants are found for N122 and E123. This allowed greater flexibility of the ligating atoms in these residues, yielding closer distances to the metal centre during the MD simulations,

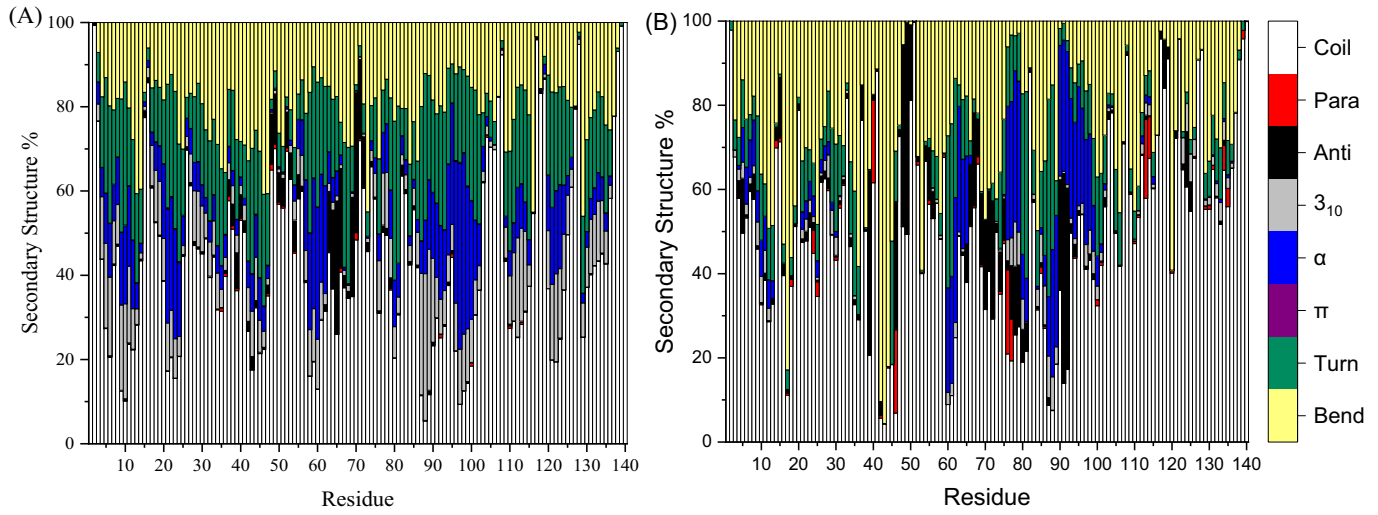

Fig. 9. Secondary structure distribution per residue after 1.80 μs aMD of the (A) free and (B) Cu(II)-αS. The β-sheets are denoted with red (parallel) and black (antiparallel), and the α-helices with grey (3_{10}), blue (α) and purple (π). (For interpretation of the references to colour in this figure legend, the reader is referred to the web version of this article.)

Table 5
Detailed secondary structure percentages of the three main regions of αS.

Region	β character (%)	α character (%)	Other (%)
free-αS			
N-terminal	2.12	16.30	81.58
NAC	6.84	14.56	78.61
C-terminal	0.26	18.05	81.69
Cu(II)-αS			
N-terminal	2.45	9.73	87.82
NAC	5.10	14.73	80.18
C-terminal	0.26	14.30	85.44

Table 6
Secondary structure percentages for the free and copper-bound peptide systems.

	β character (%)	α character (%)	Other (%)
free-αS	2.47	16.55	80.98
Cu(II)-αS	2.23	12.43	85.33

albeit with more fluctuations in the bond distance, compared to the other coordinating atoms, Table S3. The stability of the distance of atoms in the metal-coordination sites, can be seen from Fig. S2, where the distances are maintained within bonding length; even for the O from Asn122, where the lowest force constant is seen, the bond distance is seen fluctuating at a high degree at the beginning of one out of the three trajectories.

3.2. Accelerated MD on free and copper-bound αS

The MD simulations presented here were performed using the ff03ws force field in combination with the OBC implicit solvent. The evaluation of the folding characteristics in the simulations of the metal-free system against experimental evidence, Table 2, suggested the suitability of this combination for the simulation of αS over alternative force fields and explicit solvents, as seen in our previous assessment of such systems [44]. From the survey presented in that table, it can be seen that there is no collective agreement in the literature regarding the folding characteristics of this peptide, even within each of the studies, in certain cases reporting a great potential deviation from their reported secondary structure percentages. We do, however, see good agreement between our calculated values and those from the ATR-FTIR experiment [77], where a 3% β-sheet character is reported and with the helicity at 35%. A more in-depth discussion of our results on the secondary structures of the simulated systems is given further below. Additionally to the secondary structure propensities reported in the experiments cited below, we further include a comparison of Cα chemical shifts, Fig. 3, where we find a mean deviation of 1.42% from experiment, hinting towards a great similarity in the local covalent interactions of the experimental and simulated systems. Considering these remarks, we are confident in the capacity of our chosen force field and solvent in providing accurate predictions of the two systems we examine.

Equilibration of the MD simulations performed here, was assessed from the RMSD plots, given in Fig. 4, with the cumulative average settling to a plateau, despite the fluctuations observed in the RMSD values over the length of the simulations. This, along with the length of the cMD trajectories, where the aMD simulations were extended from, are enough to ascertain the stability of the systems.

Analysis of the Cu(II) coordination sites (Fig. S2, Table S2 and Table S3) confirm that Cu-L distances and L-Cu-L angles are stable over the course of the entire trajectory. For the assessment of the most prominent geometry expressed by the peptide, clusters were created using the cartesian coordinates of the Cα – the different clusters are given in Table S5. The coordination of ligating atoms in each of the metal sites, from the average cluster structure obtained from cartesian PCA analysis, is shown below.

The conformational assembly of the metal sites, seen in Fig. 5 and Table S4, correlates with experimental observations, detecting a distorted square planar arrangement of atoms, with the high affinity N-terminal coordination site maintaining a geometry that is not strongly distorted from idealised square planar [8,20,22,85]. Interaction with atoms neighbouring the ligands, distorts the geometry in each of the sites, exerting repulsion on the equatorial positions. These atoms are from a sidechain oxygen of Glu35, and the second oxygen in the Glu123 sidechain. The coordination of Asp2 in a bidentate fashion, adds to the strain on the geometry of the first metal site, further distorting the square planar geometry.

R_g values over the aMD trajectories, are shown in Fig. 6, along with the cumulative average. The rolling standard deviation (with a 25 ns window) of the simulations were also plotted, Fig. S3, showing change of SD over time, providing further evidence of equilibration over the course of each run. From these plots, it is evident that the system fluctuates between a range of R_g values, with a SD for the free peptide of 4.58 Å and for the copper-bound at 4.31 Å. The distribution plots of the

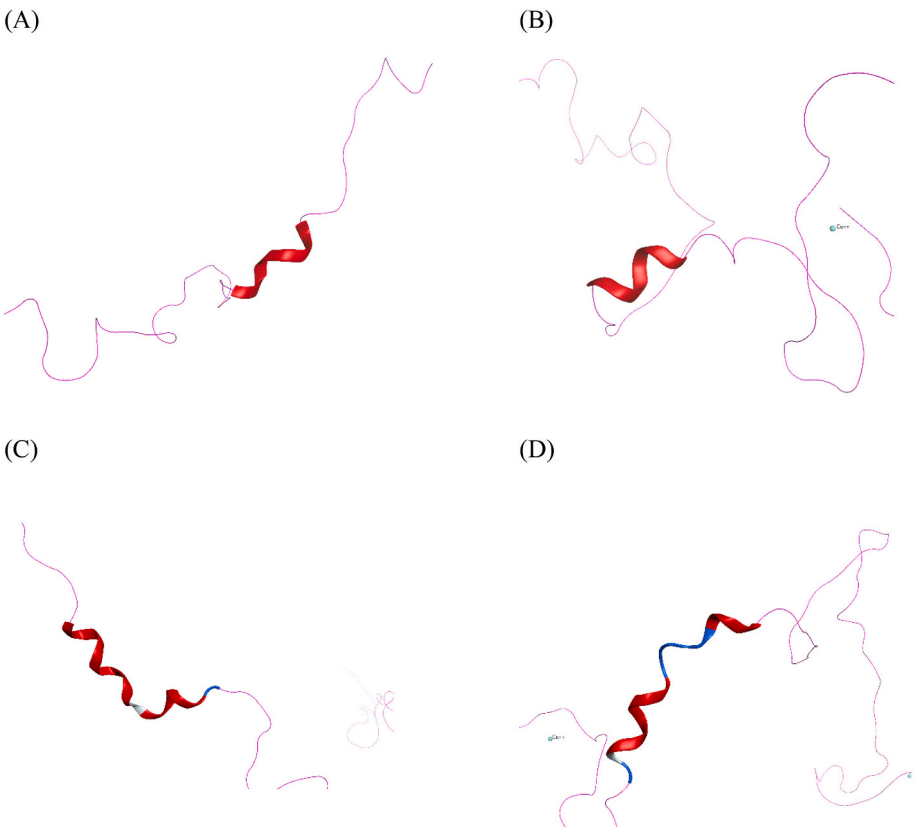

Fig. 10. Representation of the most populated α-helical regions (red), between residues 57–62 in the (A) unbound and (B) Cu(II)-bound αS and respectively (C—D) between residues 87–101. (For interpretation of the references to colour in this figure legend, the reader is referred to the web version of this article.)

R_g for each of the runs, are given in Fig. S4, where all runs are seen exhibiting peak values close to the average; thus presenting three correlating trajectories, for each system.

Upon comparison of the R_g data, an overall increase in the compactness of the peptide is seen upon metal ion binding, with the Cu (II)-αS being 4.5 Å smaller when compared to the free-αS. The standard deviation in Rg, as well as maximum and minimum values, are also smaller in the Cu-bound peptide, indicating a more compact and less flexible trajectory in the presence of two metal ions. This comes as a result of the closer contacts developed within the peptide, especially from the macro-chelation formed with the coordination of the first two residues and His50 in the first metal site. This increase in the intramolecular interactions is seen not only in the Cα contact maps (*vide infra* Fig. 15), but also in the slightly increased sphericity of the copper-coordinated system, Table S6. The sphericity of the system was assessed after calculating the globularity, by dividing the smallest by the largest diagonalized eigenvalues of the R_g tensor, whereby *Globularity* = λ_x/λ_z. This is also seen at the free energy landscape of R_g against globularity, Fig. 7, where the free peptide, although visiting conformations up to 0.5, on average displayed lower globularity values. The copper-bound peptide appears to have a more constrained sampling of the conformational space, owing to the increased ordering of residues bound to metal centres, decreasing flexibility of the overall system.

A significant contribution to the secondary structural characteristics of αS is attributed in or around motifs of repeating residue regions KTK (E/Q)GV, found between residues 32–37, 43–48 and 58–63. These repeats start in the N-terminus and extend into the NAC region of αS, and have been implicated before to be involved in the ordered arrangement of the peptide [86–88]. Within these repeats, β-hairpin structures have been found in aMD trajectories for both the unbound and metal-bound peptide, corroborating the results found by Yu et al. [89], on the region where these are observed (residues 38–53) through the formation of anti-parallel β-sheets; Fig. 8 shows the presence of these folding elements from the clustered structures. An experimental study looking at the nucleation capacities of different regions within α-Synuclein, has reported the region encompassing residues 37–61 to act as a nucleation-promoter, possibly as a result of the β-hairpin assemblies [90]. More recently, Y39 has been the focus of an experimental study, that concluded in the importance of the aromaticity in the folding mechanics of that region of the peptide [91]. Here, we find that these structures appear more frequently in the Cu(II)-bound α-Synuclein trajectory compared to the unbound one, Fig. S5 and Fig. S6. Another region where β-hairpin structures have been found here, is between residues 63–72, expressed almost in twice as many frames as in the hairpin found between residues 38–53. The maximum time these have been found to last in each of the cases, are given in Table 4, with the copper-bound system exhibiting the greatest persistency in both of these regions. Potential intramolecular interactions, such as salt bridges between lysine and glutamine residues within these repeats, are discussed in more detail below.

The secondary structure characteristics of the peptide are shown in Fig. 9, Table 5 and Table 6. The amounts of the different structures in the systems indicate the ratio of β-characteristics in the different regions of the peptide remains consistent with experimental observations, with the highest percentage of sheets present in the NAC region [92]. Despite the lack of experimental data on the secondary characteristics of the copper-bound peptide, an in-depth evaluation of the free peptide, simulated here, has been given both in our past works [44], as well as the introduction of this section, with experimental findings from CD [78–81], Raman [82,83] and ATR-FTIR [77] spectroscopic techniques, and NMR data on the chemical shifts of the Cα within this system [84]. Our findings showed agreement with values reported from the ATR-FTIR study (α-helices: 35%; β-sheets: 3%) [77], and α-helical percentages reported from CD experiments (α-helices: 19 ± 1% [81] and 22.5 ±

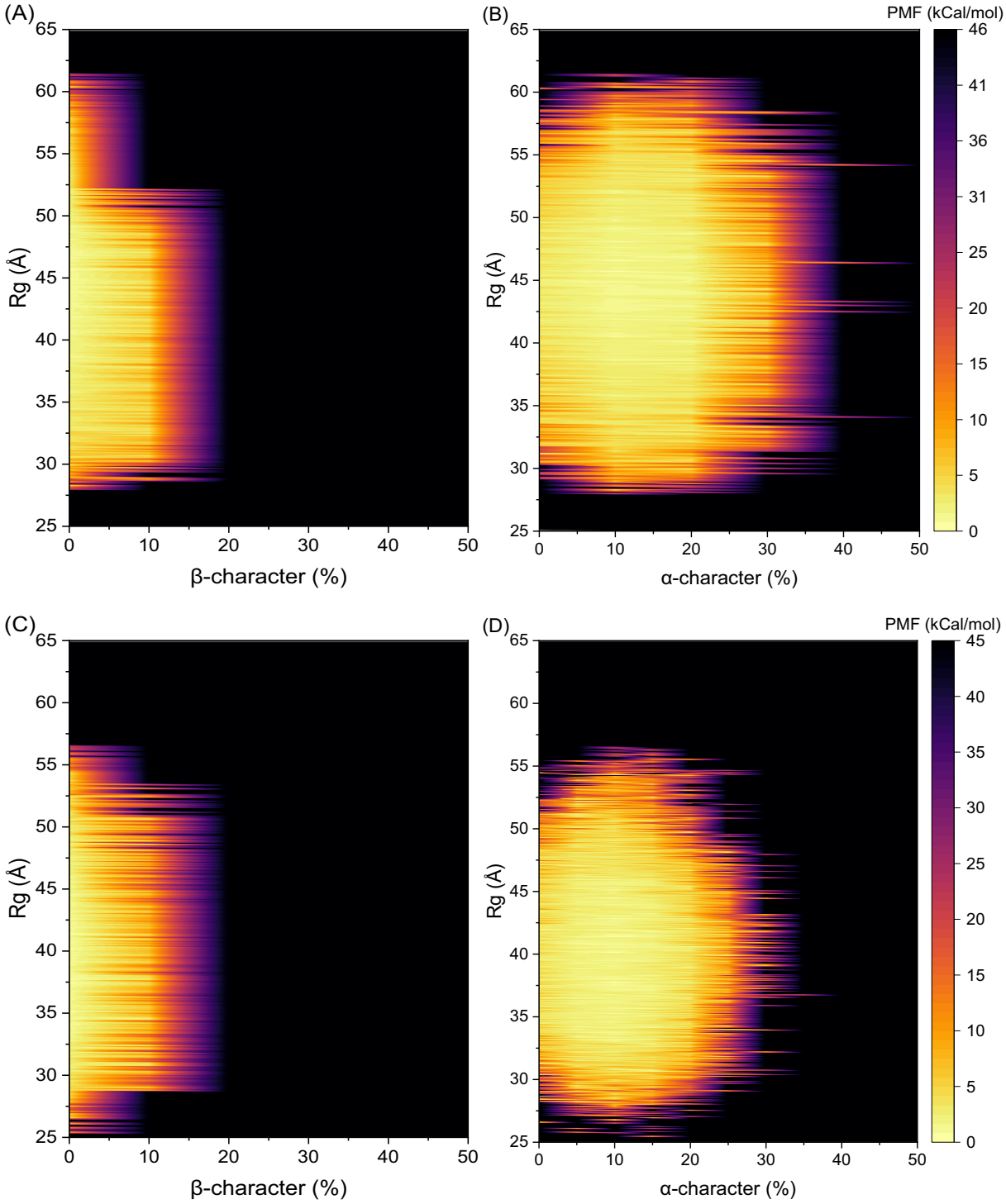

Fig. 11. Free energy landscape plots of R_g against α- and β-characteristics present in the (A-B) unbound and (C—D) Cu(II)-bound peptide.

1.5% [80]). The level of agreement between the free-peptide secondary structure found here and the experimental values, permits the assessment of the differences between the two systems, with relative confidence in their reliability. The NAC region of the peptide has long been thought to be involved in the pathogenesis of PD, owing to the formation a hydrophobic β-sheet intermediate in that particular region [93]. The secondary structure in NAC is almost unaffected by binding of Cu(II), with a decrease in β-sheet, possibly owing to the pull exerted on the residues comprising the NAC region, from coordination of His50 to Cu (II), but also from the increased preference for long-range interactions, upon binding of the metal ion, seen both in the increased compactness of the system, Fig. 15 and Table 3, but also in the lack of 3_{10}-helices, as opposed to the metal-free peptide, where such structures make up most of the α-character in the system.

Conversely, a decrease in the α-helical character is observed in the residues involved in the copper interactions, in both N- and C-termini. This decreased helicity, may in turn influence the membrane binding affinity of the peptide, especially considering the higher affinity lipid membrane binding region is in the N-terminus [94]. Experimental evidence have also reported oxidation of Met residues in that region of the

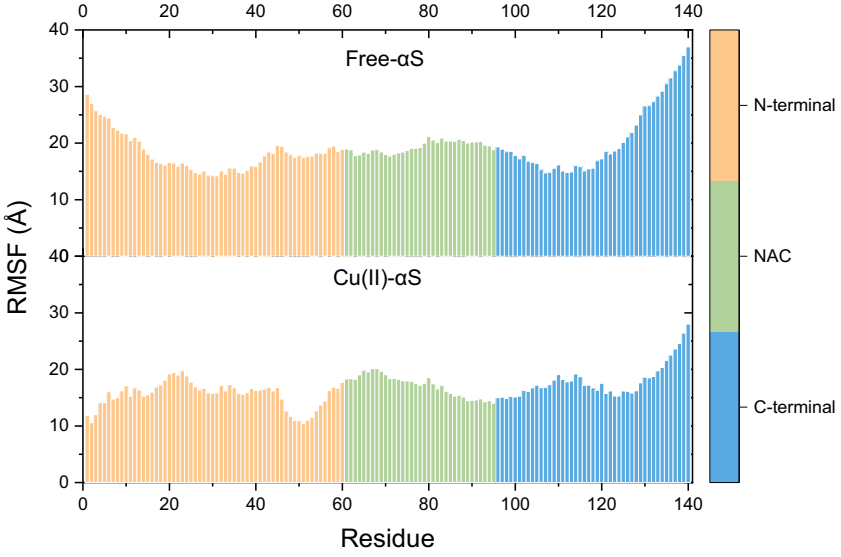

Fig. 12. Root mean square fluctuation, of the individual residues in each of the systems.

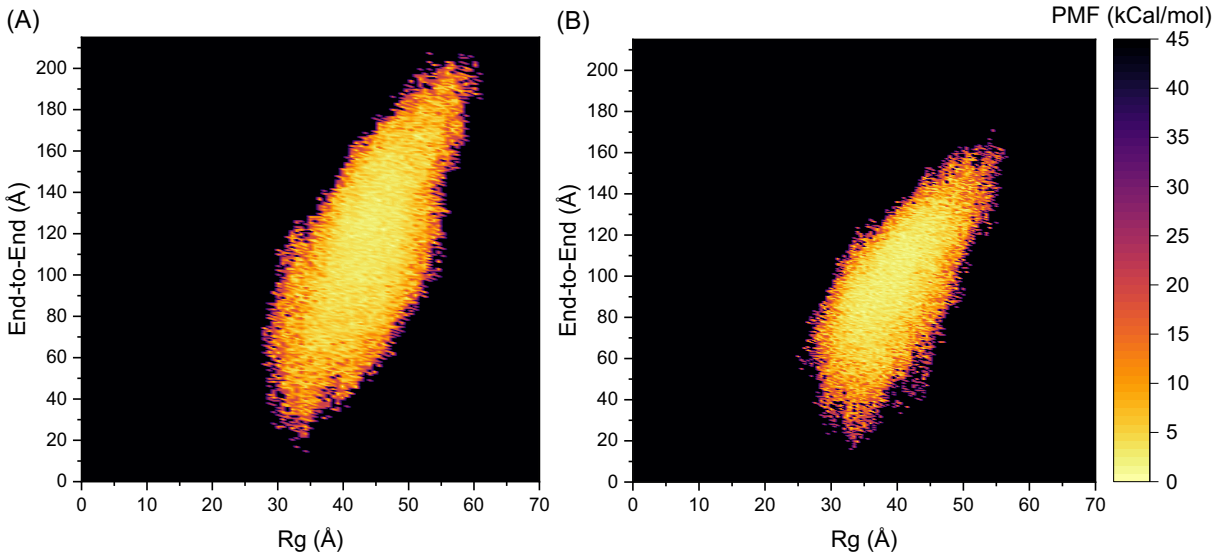

Fig. 13. 2D free energy plot of the end-to-end distance against the radius of gyration (R_g), from the aMD simulations on the (A) free and (B) copper-bound peptide.

peptide results in a decreased membrane affinity [95,96], as well as the possible modulation of αS, as a result of protein interactions in that region [97]. This drop in the percentage of α-helices, particularly in the N-terminus of the Cu(II)-αS system, suggests the possible hampering of the binding affinity with lipid membranes upon coordination of the metal-ion, as this region has generally been linked with the ability of αS to form such interactions [98], aiding in the physiological activity of αS and as a way of balancing between the normal and aberrant forms [99]. The dampening of these interactions in the Cu(II)-coordinated system may therefore act as a mechanism for the formation of toxic oligomers. The community is divided on the possible effects of membrane coordination, with arguments on both sides: regulation of misfolding and oligomerization upon membrane binding [100], and promotion of aggregation [101]. Since we do not study the membrane interactions of these systems here, as well as the documented effect of membrane curvature [102], these can only act as speculations on the possible effects when these systems do in fact bind. We would therefore direct readers to a recently published experimental study on the possible mechanisms that take place upon interaction of αS with lipid membranes in the presence of Cu(II), where two possible hypothesis are presented: (1) an increased affinity of Cu(II) interactions to the N-terminal of monomeric αS, thus increasing oligomerization in-solution and decreasing upon membrane-binding; (2) free-αS membrane binding results in extended helical formation increasing the affinity of Cu(II) association with the C-terminal binding site [94].

A closer evaluation of helical characteristics implicates residues Glu57-Gln62 and Ser87-Gly101 as the regions with most helical population, in both the unbound and Cu(II)-bound peptides. The latter region was found to exhibit the greatest mean α-character occupancy both in the free, at 38.31%, and Cu(II)-αS, at 38.61%, while the former region presented mean occupancies of 34.55% and 33.18%, respectively. Representations of the structure in each of these regions is given in Fig. 10. A thing to note here is that the region between residues Ser87-Gly101 is split between residues Ala91-Phe94, by coiled structures, resulting in two short helices between residues Ser87-Ala90 and Val95-Leu100. This happens for the majority of the conformations, despite instances of a long continuous helix, steric hindrance restricts the conservation of such structures. The observations here are in line with

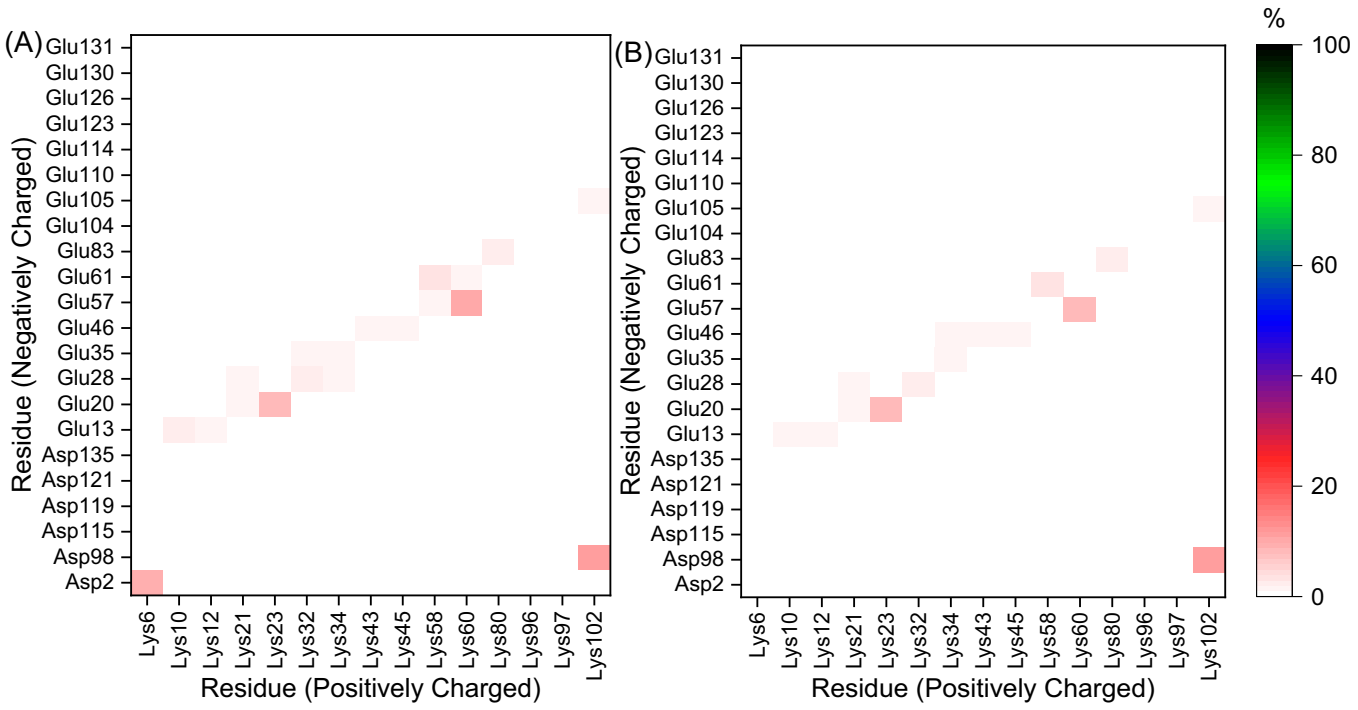

Fig. 14. Salt bridges formed between negatively and positively charged residues in (A) free and (B) copper-bound α-Synuclein.

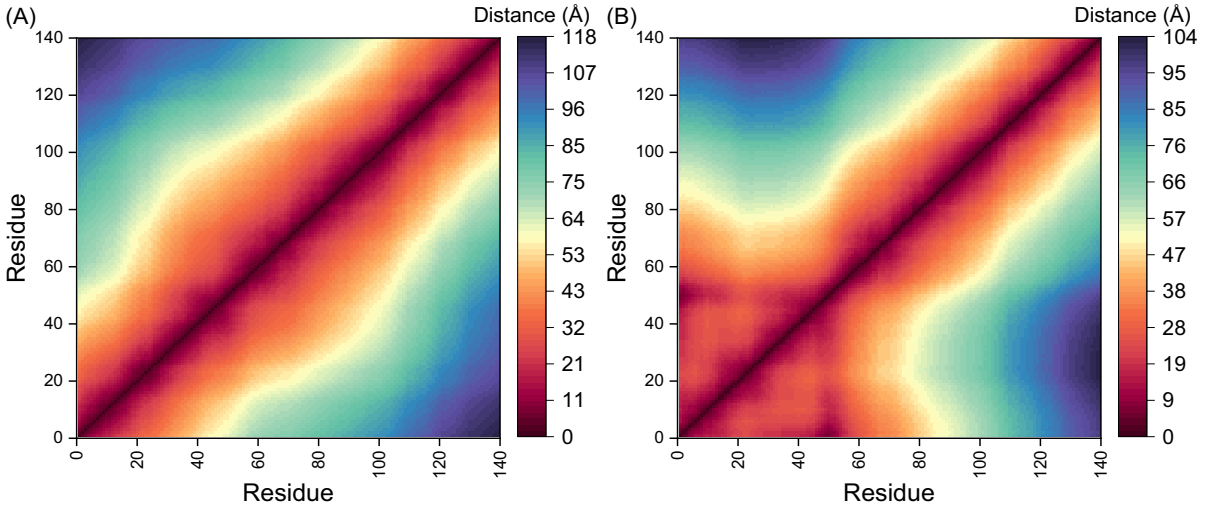

Fig. 15. Contact maps of the alpha-C from the dynamics of the (A) free and (B) Cu(II)-bound peptide.

experimental results, suggesting the importance of the central NAC region in fibrillation of αS, having the first major helical region occupying the border of the N-terminal, extending to the NAC region, and the second starting in the NAC and extending in the C-terminal.

The two regions reported above, represent the two most populated helical regions, occurring around at least 1/3rd of the total trajectory, and at least consist of 6 residues. A further four regions where notable helices occur between 4 residues are found in: Ser9-Lys12[1] (free-αS: 35.50%; Cu(II)-αS: 24.13%), Glu20-Thr23 (free-αS: 35.00%; Cu(II)-αS: 22.83%), Gly111-Glu114 (free-αS: 29.36%; Cu(II)-αS: 28.66%), Pro120-Glu123 (free-αS: 35.07%; Cu(II)-αS: 0.48%). Thus, our data suggests an increased presence of helices in the N-terminal, but an overall decrease of these structures, as a result of the Cu(II) coordination.

Below, Fig. 11, displays the reweighted free energy landscape of R_g *vs.* two elements of secondary structure characteristics in the two systems. The potential of mean force (PMF) energies in Fig. 11, display the lowest values at 0% β-character, with *ca.* 16% and 10% α-character, for the free and copper-bound systems, respectively. The free peptide may also be seen sampling a greater conformational space, as explained before, possibly due to the increased flexibility of the system. The local minima with the lowest energy values appear to be between R_g values 35–45 Å in both cases, something to be expected considering the experimental and average R_g values, shown above.

The flexibility of each residue is shown by their root mean square fluctuation (RMSF), Fig. 12. From that, it is evident that adding the

[1] This region may be further extended to include residues Phe4-Leu8, resulting in an overall helical population of 29.65% for the free-αS and 16.92% for the Cu(II)-αS system.

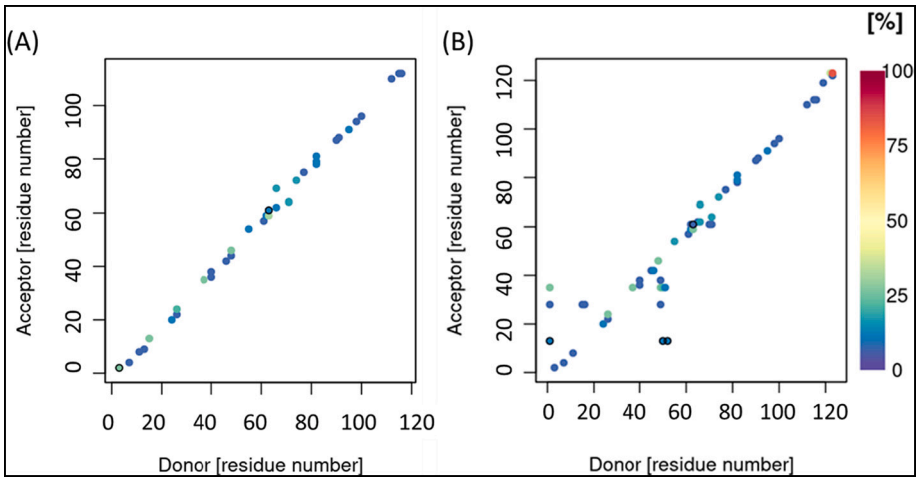

Fig. 16. Hydrogen bonds present of the (A) free and (B) copper-bound peptide.

metal ions to the peptide restricted the motion of the residues in the N-terminal, while the mobility of His50 and neighbouring residues is also reduced. This is due to the macro-chelation of Cu(II) by N-terminal residues and His50, in which the metal ion restricts the motion of neighbouring residues. In contrast, metal ion binding does not strongly affect the motion of NAC or C-terminal residues: indeed, RMSF of the Cu (II) bound system is actually higher in metal binding residues when compared to the free peptide. However, the very large RMSF seen at the C-terminus is reduced from almost 40 Å to below 30 Å when Cu(II) is bound.

The free energy landscape associated with a combination of R_g and end-to-end distance, Fig. 13, illustrates the smaller size found in the Cu (II)-αS, when compared to the unbound peptide, with the former exploring conformations where the end-to-end distance was maintained below 165 Å, with an average of 97.5 ± 20.6 Å, as opposed to the free peptide, which went as high as 210 Å, averaging 117.1 ± 27.2 Å.

In the intramolecular interactions of the two systems, binding of two Cu(II) ions does not strongly alter the pattern of salt bridges within the peptide, Fig. 14. The sole exception is Asp2, which is bound directly to copper and so is not available for interaction with Lys6. This is true even for the repeat sequences where hairpins were observed, highlighting the transience of these elements of secondary structure. Hydrogen bonds are more strongly affected by metal ions (Fig. 16), especially in the N-terminal region, where a significant number of "off-diagonal" H-bonds are found in the Cu(II)-bound form. This again appears to be related to the macro-chelation of Cu(II), which brings His50 and neighbouring residues into close contact with N-terminal ones, closely interacting with residues Glu35 and Glu13. As a result of these contacts, neighbouring residues to His50 are also seen forming H-bonds with more distanced ones, such as Val49-Glu35 and Met1-Glu35. The most significant hydrogen bond formed in the copper-bound system, is seen intra-residue in Glu123 (at *ca.* 83% of frames). This is also evident in maps of close contacts between residues (Fig. 15): the free peptide only shows contact close to the diagonal, but the Cu(II)-bound peptide has close contact throughout the N-terminal region, extending as far as residue 70, *i.e.* into the NAC. It should be noted, however, that the intrinsically disordered nature of α-Synuclein means that occupancy of all salt-bridge and hydrogen bond contacts is low, typically under 10% of the overall trajectory.

Research on the behaviour of α-Synuclein in its monomeric form has shown that it adopts no lasting secondary characteristics, instead they are rather transient, owing to its natively disordered nature, favoring unfolded and extended conformations [82,103]. The role of copper ions in the aggregation propensity of α-Synuclein has been studied extensively in the scientific community, with evidence suggesting that it induces aggregation of the peptide [12]. This could be attributed, in part, to restriction of the peptide's structure, allowing it to maintain the folded conformation when interacting with the metal ions, possibly owing to the restriction in flexibility introduced by metal coordination [104]. Evidence for this may be seen in the increased contacts between the residues, Fig. 15, presenting a more populated region where the Cu(II)-interactions occur. The R_g data from the accelerated MD simulations, provide further evidence of this upon binding of two Cu(II) ions, showing a decrease in the R_g of 4.5 Å. The secondary structure characteristics exhibit a decrease in defined characteristics going from the unbound peptide to Cu(II)-αS, show that the compactness gain in the bound peptide is a direct result of the binding to the metal ions, increasing the intramolecular interactions, as evident by the increased presence of hydrogen bonds, Fig. 16.

4. Conclusions

The effect of copper ions on the structure of the peptide has not been extensively studied computationally. Analysis of aMD trajectories, encompassing radius of gyration, RMSF and secondary structure, provide evidence of an average increased compactness and rigidity of the peptide upon the binding of two copper ions at the sites established by experimental studies. The data collected here corroborates previous reports that suggest an increase in stabilization of folding characteristics upon the binding of Cu(II) to αS, seen here from the RMSF and R_g of the copper-coordinated system, exhibiting a decreased flexibility, despite the lower amount of secondary structure present [9]. The more prominent α-helical character in the C-terminus of the free peptide, has been reported before [105] and also seen in the present work, although this is reduced in the copper-bound system, possibly owing to the coordination of the metal ion with residues in this site.

The contribution of the KTKEGV repeats, extending from the N-terminal region into the NAC, in the secondary structure and thus folding of the peptide has also been reported here and validates past observations [86]. Two β-hairpin regions have also been found here, between residues 38–53 and 63–72, with the former being sustained for longer, especially where the 38–53 residues are concerned, in the Cu(II)-bound peptide, where they are maintained for up to *ca.* 72 consecutive ns, as opposed to the *ca.* 42 ns in the unbound one. Copper binding leads to loss of some β-characteristics in the NAC region, when compared to the unbound, possibly owing to the macro-chelation of a copper ion in the N-terminal region, restricting the adoption of a folded conformation in the neighbouring region. The RMSF of the residues involved in the copper ion interactions are significantly reduced, decreasing from *ca.* 20–30 Å to 10 Å in the N-terminal and from *ca.* 40 Å to 30 Å in the C-terminal. The effect of binding two Cu(II) ions on the RMSF appears to carry changes in the NAC region, restricting the motion of the constituting residues by 5

Å. The higher flexibility of the free peptide is also evident from the free energy landscape plots of globularity and end-to-end distances, showing a greater conformational space explored by the unbound peptide, as well as reaching more spherical conformations compared to the copper-bound case.

Declaration of Competing Interest

The authors confirm that no conflict of interest exists in this work.

Data availability

Data will be made available on request.

Acknowledgements

We acknowledge the role of Advanced Research Computing @ Cardiff (ARCCA) in providing computational resources for simulations.

JAP and LS designed simulations; LS performed simulations and analysed data; LS and JAP wrote the manuscript.

Appendix A. Supplementary data

Supplementary data to this article can be found online at https://doi.org/10.1016/j.jinorgbio.2022.112068.

References

[1] M. Goedert, R. Jakes, M.G. Spillantini, The synucleinopathies: twenty years on, J. Parkinsons Dis. 7 (2017) S53–S71.
[2] K. Uéda, H. Fukushima, E. Masliah, Y.U. Xia, A. Iwai, M. Yoshimoto, D.A. C. Otero, J. Kondo, Y. Ihara, T. Saitoh, Molecular cloning of cDNA encoding an unrecognized component of amyloid in Alzheimer disease, Proc. Natl. Acad. Sci. U. S. A. 90 (1993) 11282–11286.
[3] V.N. Uversky, Unusual biophysics of intrinsically disordered proteins, Biochim. Biophys. Acta, Proteins Proteomics 1834 (2013) 932–951.
[4] C.J. Oldfield, A.K. Dunker, Intrinsically disordered proteins and intrinsically disordered protein regions, Annu. Rev. Biochem. 83 (2014) 553–584.
[5] V.N. Uversky, J. Li, A.L. Fink, Evidence for a partially folded intermediate in α-synuclein fibril formation, J. Biol. Chem. 276 (2001) 10737–10744.
[6] B. Ahmad, Y. Chen, L.J. Lapidus, Aggregation of α-synuclein is kinetically controlled by intramolecular diffusion, Proc. Natl. Acad. Sci. U. S. A. 109 (2012) 2336–2341.
[7] V.N. Uversky, J. Li, A.L. Fink, Metal-triggered structural transformations, aggregation, and fibrillation of human α-synuclein: a possible molecular link between parkinson's disease and heavy metal exposure, J. Biol. Chem. 276 (2001) 44284–44296.
[8] R.M. Rasia, C.W. Bertoncini, D. Marsh, W. Hoyer, D. Cherny, M. Zweckstetter, C. Griesinger, T.M. Jovin, C.O. Fernández, Structural characterization of copper (II) binding to α-synuclein: insights into the bioinorganic chemistry of Parkinson's disease, Proc. Natl. Acad. Sci. U. S. A. 102 (2005) 4294–4299.
[9] S.R. Paik, H.J. Shin, J.H. Lee, C.S. Chang, J. Kim, Copper(II)-induced self-oligomerization of α-synuclein, Biochem. J. 340 (1999) 821–828.
[10] A. Binolfi, R.M. Rasia, C.W. Bertoncini, M. Ceolin, M. Zweckstetter, C. Griesinger, T.M. Jovin, C.O. Fernández, Interaction of α-synuclein with divalent metal ions reveals key differences: a link between structure, binding specificity and fibrillation enhancement, J. Am. Chem. Soc. 128 (2006) 9893–9901.
[11] A. Binolfi, L. Quintanar, C.W. Bertoncini, C. Griesinger, C.O. Fernández, Bioinorganic chemistry of copper coordination to alpha-synuclein: relevance to Parkinson's disease, Coord. Chem. Rev. 256 (2012) 2188–2201.
[12] X. Wang, D. Moualla, J.A. Wright, D.R. Brown, Copper binding regulates intracellular alpha-synuclein localisation, aggregation and toxicity, J. Neurochem. 113 (2010) 704–714.
[13] D.R. Brown, Oligomeric alpha-synuclein and its role in neuronal death, IUBMB Life 62 (2010) 334–339.
[14] S.R. Paik, H.J. Shin, J.H. Lee, Metal-catalyzed oxidation of α-synuclein in the presence of copper(II) and hydrogen peroxide, Arch. Biochem. Biophys. 378 (2000) 269–277.
[15] J.A. Wright, D.R. Brown, Alpha-synuclein and its role in metal binding: relevance to Parkinson's disease, J. Neurosci. Res. 86 (2008) 496–503.
[16] C. Wang, L. Liu, L. Zhang, Y. Peng, F. Zhou, Redox reactions of the α-synuclein-Cu2+ complex and their effects on neuronal cell viability, Biochemistry 49 (2010) 8134–8142.
[17] R. Ramis, J. Ortega-Castro, B. Vilanova, M. Adrover, J. Frau, Cu2+, Ca2+, and methionine oxidation expose the hydrophobic α-synuclein NAC domain, Int. J. Biol. Macromol. 169 (2021) 251–263.
[18] F. Rose, M. Hodak, J. Bernholc, Mechanism of copper(II)-induced misfolding of Parkinson's disease protein, Sci. Rep. 1 (2011) 1–5.
[19] Y.H. Sung, C. Rospigliosi, D. Eliezer, NMR mapping of copper binding sites in alpha-synuclein, Biochim. Biophys. Acta, Proteins Proteomics 1764 (2006) 5–12.
[20] S.C. Drew, L.L. Su, C.L.L. Pham, D.J. Tew, C.L. Masters, L.A. Miles, R. Cappai, K. J. Barnham, Cu2+ binding modes of recombinant α-synuclein - insights from EPR spectroscopy, J. Am. Chem. Soc. 130 (2008) 7766–7773.
[21] D.R. Brown, Metal binding to alpha-synuclein peptides and its contribution to toxicity, Biochem. Biophys. Res. Commun. 380 (2009) 377–381.
[22] R. Ramis, J. Ortega-Castro, B. Vilanova, M. Adrover, J. Frau, Copper(II) binding sites in N-terminally acetylated α-synuclein: a theoretical rationalization, J. Phys. Chem. A 121 (2017) 5711–5719.
[23] R. Ramis, J. Ortega-Castro, R. Casasnovas, L. Marino, B. Vilanova, M. Adrover, J. Frau, A coarse-grained molecular dynamics approach to the study of the intrinsically disordered protein α-Synuclein, J. Chem. Inf. Model. 59 (2019) 1458–1471.
[24] Z. Cao, L. Liu, L. Zhao, H. Li, J. Wang, Comparison of the structural characteristics of Cu2+−bound and unbound α-syn12 peptide obtained in simulations using different force fields, J. Mol. Model. 19 (2013) 1237–1250.
[25] J.A. Wright, X. Wang, D.R. Brown, Unique copper-induced oligomers mediate alpha-synuclein toxicity, FASEB J. 23 (2009) 2384–2393.
[26] D.R. Brown, Interactions between metals and α-synuclein - function or artefact? FEBS J. 274 (2007) 3766–3774.
[27] F. Camponeschi, D. Valensin, I. Tessari, L. Bubacco, S. Dell'Acqua, L. Casella, E. Monzani, E. Gaggelli, G. Valensin, Copper(I)-α-synuclein interaction: structural description of two independent and competing metal binding sites, Inorg. Chem. 52 (2013) 1358–1367.
[28] D. Valensin, F. Camponeschi, M. Luczkowski, M.C. Baratto, M. Remelli, G. Valensin, H. Kozlowski, The role of His-50 of α-synuclein in binding cu(ii): PH dependence, speciation, thermodynamics and structure, Metallomics 3 (2011) 292–302.
[29] A. Villar-Piqué, G. Rossetti, S. Ventura, P. Carloni, C.O. Fernández, T.F. Outeiro, Copper(II) and the pathological H50Q α-synuclein mutant: environment meets genetics, Commun. Integr. Biol. 10 (2017) 1–4.
[30] C.G. Dudzik, E.D. Walter, B.S. Abrams, M.S. Jurica, G.L. Millhauser, Coordination of copper to the membrane-bound form of α-synuclein, Biochemistry 52 (2013) 53–60.
[31] H.R. Lucas, J.C. Lee, Copper(ii) enhances membrane-bound α-synuclein helix formation, Metallomics 3 (2011) 280.
[32] C.G. Dudzik, E.D. Walter, G.L. Millhauser, Coordination features and affinity of the Cu2+ site in the α-synuclein protein of Parkinson's disease, Biochemistry 50 (2011) 1771–1777.
[33] A. Ahmad, C.S. Burns, A.L. Fink, V.N. Uversky, Peculiarities of copper binding to α-synuclein, J. Biomol. Struct. Dyn. 29 (2012) 825–842.
[34] M. Bortolus, M. Bisaglia, A. Zoleo, M. Fittipaldi, M. Benfatto, L. Bubacco, A. L. Maniero, Structural characterization of a high affinity mononuclear site in the copper(II)-α-synuclein complex, J. Am. Chem. Soc. 132 (2010) 18057–18066.
[35] R. De Ricco, D. Valensin, S. Dell'Acqua, L. Casella, P. Dorlet, P. Faller, C. Hureau, Remote His50 acts as a coordination switch in the high-affinity N-terminal centered copper(II) site of α-synuclein, Inorg. Chem. 54 (2015) 4744–4751.
[36] T.S. Choi, J. Lee, J.Y. Han, B.C. Jung, P. Wongkongkathep, J.A. Loo, M.J. Lee, H. I. Kim, Supramolecular modulation of structural polymorphism in pathogenic α-synuclein fibrils using copper(II) coordination, Angew. Chem. Int. Ed. 57 (2018) 3099–3103.
[37] S.C. Drew, The N terminus of α-synuclein forms cu II -bridged oligomers, Chem. A Eur. J. 21 (2015) 7111–7118.
[38] D.L. Abeyawardhane, D.R. Heitger, R.D. Fernández, A.K. Forney, H.R. Lucas, C-terminal Cu II coordination to α-synuclein enhances aggregation, ACS Chem. Neurosci. 10 (2019) 1402–1410.
[39] A. Villar-Piqué, T.L. Da Fonseca, R. Sant'Anna, É.M. Szegö, L. Fonseca-Ornelas, R. Pinho, A. Carija, E. Gerhardt, C. Masaracchia, E.A. Gonzalez, G. Rossetti, P. Carloni, C.O. Fernández, D. Foguel, I. Milosevic, M. Zweckstetter, S. Ventura, T. F. Outeiro, Environmental and genetic factors support the dissociation between α-synuclein aggregation and toxicity, Proc. Natl. Acad. Sci. U. S. A. 113 (2016). E6506–E6515.
[40] S.Y. Mandaci, M. Caliskan, M.F. Sariaslan, V.N. Uversky, O. Coskuner-Weber, Epitope region identification challenges of intrinsically disordered proteins in neurodegenerative diseases: secondary structure dependence of α-synuclein on simulation techniques and force field parameters, Chem. Biol. Drug Des. 96 (2020) 659–667.
[41] P. Li, K.M. Merz, MCPB.py: a python based metal center parameter builder, J. Chem. Inf. Model. 56 (2016) 599–604.
[42] R.B. Best, W. Zheng, J. Mittal, Balanced protein-water interactions improve properties of disordered proteins and non-specific protein association, J. Chem. Theory Comput. 10 (2014) 5113–5124.
[43] D. Song, R. Luo, H.-F. Chen, The IDP-specific force field ff14IDPSFF improves the conformer sampling of intrinsically disordered proteins, J. Chem. Inf. Model. 57 (2017) 1166–1178.
[44] L. Savva, J.A. Platts, Evaluation of implicit solvent models in molecular dynamics simulation of α-synuclein, J. Biomol. Struct. Dyn. 1–16 (2022).
[45] K.B. Pedersen, J.C. Flores-Canales, B. Schiøtt, Predicting molecular properties of α-synuclein using force fields for intrinsically disordered proteins, Proteins (2022), https://doi.org/10.1002/prot.26409.
[46] M.C. Ahmed, L.K. Skaanning, A. Jussupow, E.A. Newcombe, B.B. Kragelund, C. Camilloni, A.E. Langkilde, K. Lindorff-Larsen, Refinement of α-synuclein

ensembles against SAXS data: comparison of force fields and methods, Front. Mol. Biosci. 8 (2021) 1–13.
[47] O. Palomino-Hernandez, C. Santambrogio, G. Rossetti, C.O. Fernandez, R. Grandori, P. Carloni, Molecular dynamics-assisted interpretation of experimentally determined intrinsically disordered protein conformational components: the case of human α-synuclein, J. Phys. Chem. B 126 (2022) 3632–3639.
[48] P. Robustelli, S. Piana, D.E. Shaw, Developing a molecular dynamics force field for both folded and disordered protein states, Proc. Natl. Acad. Sci. U. S. A. 115 (2018) E4758–E4766.
[49] M. Sandal, F. Valle, I. Tessari, S. Mammi, E. Bergantino, F. Musiani, M. Brucale, L. Bubacco, B. Samorì, Conformational equilibria in monomeric α-synuclein at the single-molecule level, PLoS Biol. 6 (2008) 0099–0108.
[50] R. Corti, C.A. Marrano, D. Salerno, S. Brocca, A. Natalello, C. Santambrogio, G. Legname, F. Mantegazza, R. Grandori, V. Cassina, Depicting conformational ensembles of α-synuclein by single molecule force spectroscopy and native mass spectroscopy, Int. J. Mol. Sci. 20 (20) (2019), https://doi.org/10.3390/ijms20205181.
[51] A. Grupi, E. Haas, Segmental conformational disorder and dynamics in the intrinsically disordered protein α-synuclein and its chain length dependence, J. Mol. Biol. 405 (2011) 1267–1283.
[52] P.H. Nguyen, P. Derreumaux, Structures of the intrinsically disordered Aβ, tau and α-synuclein proteins in aqueous solution from computer simulations, Biophys. Chem. 264 (2020), 106421.
[53] P.H. Nguyen, A. Ramamoorthy, B.R. Sahoo, J. Zheng, P. Faller, J.E. Straub, L. Dominguez, J.E. Shea, N.V. Dokholyan, A. de Simone, B. Ma, R. Nussinov, S. Najafi, S.T. Ngo, A. Loquet, M. Chiricotto, P. Ganguly, J. McCarty, M.S. Li, C. Hall, Y. Wang, Y. Miller, S. Melchionna, B. Habenstein, S. Timr, J. Chen, B. Hnath, B. Strodel, R. Kayed, S. Lesné, G. Wei, F. Sterpone, A.J. Doig, P. Derreumaux, Amyloid oligomers: a joint experimental/computational perspective on Alzheimer's disease, Parkinson's disease, type II diabetes, and amyotrophic lateral sclerosis, Chem. Rev. 121 (2021) 2545–2647.
[54] A. Binolfi, E.E. Rodriguez, D. Valensin, N. D'Amelio, E. Ippoliti, G. Obal, R. Duran, A. Magistrato, O. Pritsch, M. Zweckstetter, G. Valensin, P. Carloni, L. Quintanar, C. Griesinger, C.O. Fernández, Bioinorganic chemistry of Parkinson's disease: structural determinants for the copper-mediated amyloid formation of alpha-synuclein, Inorg. Chem. 49 (2010) 10668–10679.
[55] C. Kállay, K. Várnagy, G. Micera, D. Sanna, I. Sóvágó, Copper(II) complexes of oligopeptides containing aspartyl and glutamyl residues. Potentiometric and spectroscopic studies, J. Inorg. Biochem. 99 (2005) 1514–1525.
[56] G.M. Moriarty, C.A.S.A. Minetti, D.P. Remeta, J. Baum, A revised picture of the cu (II)-α-synuclein complex: the role of N-terminal acetylation, Biochemistry 53 (2014) 2815–2817.
[57] D.A. Case, R.M. Betz, D.S. Cerutti, T.E. Cheatham, T.A. Darden, R.E. Duke, T. J. Giese, H. Gohlke, A.W. Goetz, N. Homeyer, S. Izadi, P. Janowski, J. Kaus, A. Kovalenko, T.S. Lee, S. LeGrand, P. Li, C. Lin, T. Luchko, R. Luo, B. Madej, D. Mermelstein, K.M. Merz, G. Monard, H. Nguyen, H.T. Nguyen, I. Omelyan, A. Onufriev, D.R. Roe, A. Roitberg, C. Sagui, C.L. Simmerling, W.M. Botello-Smith, J. Swails, R.C. Walker, J. Wang, R.M. Wolf, X. Wu, L. Xiao, P.A. Kollman, AMBER 2016, San Francisco, 2016.
[58] M.J. Frisch, G.W. Trucks, H.B. Schlegel, G.E. Scuseria, M.A. Robb, J. R. Cheeseman, G. Scalmani, V. Barone, B. Mennucci, G.A. Petersson, H. Nakatsuji, M. Caricato, X. Li, H.P. Hratchian, A.F. Izmaylov, J. Bloino, G. Zheng, J. L. Sonnenberg, M. Hada, M. Ehara, K. Toyota, R. Fukuda, J. Hasegawa, M. Ishida, T. Nakajima, Y. Honda, O. Kitao, H. Nakai, T. Vreven, J.A. Montgomery Jr., J. E. Peralta, F. Ogliaro, M. Bearpark, J.J. Heyd, E. Brothers, K.N. Kudin, V. N. Staroverov, R. Kobayashi, J. Normand, K. Raghavachari, A. Rendell, J. C. Burant, S.S. Iyengar, J. Tomasi, M. Cossi, N. Rega, J.M. Millam, M. Klene, J. E. Knox, J.B. Cross, V. Bakken, C. Adamo, J. Jaramillo, R. Gomperts, R. E. Stratmann, O. Yazyev, A.J. Austin, R. Cammi, C. Pomelli, J.W. Ochterski, R. L. Martin, K. Morokuma, V.G. Zakrzewski, G.A. Voth, P. Salvador, J. J. Dannenberg, S. Dapprich, A.D. Daniels, Ö. Farkas, J.B. Foresman, J.V. Ortiz, J. Cioslowski, D.J. Fox, Gaussian 09, Wallingford, CT, 2009.
[59] A.P. Scott, L. Radom, Harmonic vibrational frequencies: an evaluation of Hartree-Fock, Møller-Plesset, quadratic configuration interaction, density functional theory, and semiempirical scale factors, J. Phys. Chem. 100 (1996) 16502–16513.
[60] J.M. Seminario, Calculation of intramolecular force fields from second-derivative tensors, Int. J. Quantum Chem. 60 (1996) 1271–1277.
[61] C.I. Bayly, P. Cieplak, W.D. Cornell, P.A. Kollman, A well-behaved electrostatic potential based method using charge restraints for deriving atomic charges: the RESP model, J. Phys. Chem. 97 (1993) 10269–10280.
[62] B.H. Besler, K.M. Merz, P.A. Kollman, Atomic charges derived from semiempirical methods, J. Comput. Chem. 11 (1990) 431–439.
[63] P. Cieplak, W.D. Cornell, C. Bayly, P.A. Kollman, Application of the multimolecule and multiconformational RESP methodology to biopolymers: charge derivation for DNA, RNA, and proteins, J. Comput. Chem. 16 (1995) 1357–1377.
[64] D.A. Case, I.Y. Ben-Shalom, S.R. Brozell, D.S. Cerutti, I.T.E. Cheatham, V.W. D. Cruzeiro, T.A. Darden, R.E. Duke, D. Ghoreishi, G. Giambasu, T. Giese, M. K. Gilson, H. Gohlke, A.W. Goetz, D. Greene, R. Harris, N. Homeyer, Y. Huang, S. Izadi, A. Kovalenko, R. Krasny, T. Kurtzman, T.S. Lee, S. LeGrand, P. Li, C. Lin, J. Liu, T. Luchko, R. Luo, V. Man, D.J. Mermelstein, K.M. Merz, Y. Miao, G. Monard, C. Nguyen, H. Nguyen, A. Onufriev, F. Pan, R. Qi, D.R. Roe, A. Roitberg, C. Sagui, S. Schott-Verdugo, J. Shen, C.L. Simmerling, J. Smith, J. Swails, R.C. Walker, J. Wang, H. Wei, L. Wilson, R.M. Wolf, X. Wu, L. Xiao, Y. Xiong, D.M. York, P.A. Kollman, AMBER 2019, San Francisco, 2019.
[65] G.D. Hawkins, C.J. Cramer, D.G. Truhlar, Pairwise solute descreening of solute charges from a dielectric medium, Chem. Phys. Lett. 246 (1995) 122–129.
[66] G.D. Hawkins, C.J. Cramer, D.G. Truhlar, Parametrized models of aqueous free energies of solvation based on pairwise descreening of solute atomic charges from a dielectric medium, J. Phys. Chem. 100 (1996) 19824–19839.
[67] A. Onufriev, D. Bashford, D.A. Case, Modification of the generalized born model suitable for macromolecules, J. Phys. Chem. B 104 (2000) 3712–3720.
[68] O.C. Weber, V.N. Uversky, How accurate are your simulations? Effects of confined aqueous volume and AMBER FF99SB and CHARMM22/CMAP force field parameters on structural ensembles of intrinsically disordered proteins: amyloid-β 42 in water, Intrinsic. Disord. Proteins 5 (2017), e1377813.
[69] R.J. Deeth, N. Fey, B. Williams-Hubbard, DommiMOE: an implementation of ligand field molecular mechanics in the molecular operating environment, J. Comput. Chem. 26 (2005) 123–130.
[70] J.A. Izaguirre, D.P. Catarello, J.M. Wozniak, R.D. Skeel, Langevin stabilization of molecular dynamics, J. Chem. Phys. 114 (2001) 2090–2098.
[71] V. Kräutler, W.F.V.A.N. Gunsteren, A Fast SHAKE Algorithm to Solve Distance Constraint Equations for Small Molecules in Molecular 22, 2001, pp. 501–508.
[72] Y. Miao, W. Sinko, L. Pierce, D. Bucher, R.C. Walker, J.A. McCammon, Improved reweighting of accelerated molecular dynamics simulations for free energy calculation, J. Chem. Theory Comput. 10 (2014) 2677–2689.
[73] N.M. Glykos, Carma: a molecular dynamics analysis program, J. Comput. Chem. 27 (2006) 1765–1768.
[74] C. Andreini, G. Cavallaro, S. Lorenzini, FindGeo: a tool for determining metal coordination geometry, Bioinformatics 28 (2012) 1658–1660.
[75] D.R. Roe, T.E. Cheatham, PTRAJ and CPPTRAJ: software for processing and analysis of molecular dynamics trajectory data, J. Chem. Theory Comput. 9 (2013) 3084–3095.
[76] M. Bisaglia, I. Tessari, S. Mammi, L. Bubacco, Interaction between α-synuclein and metal ions, still looking for a role in the pathogenesis of Parkinson's disease, NeuroMolecular Med. 11 (2009) 239–251.
[77] B.A. Silva, Ó. Einarsdóttir, A.L. Fink, V.N. Uversky, Biophysical characterization of α-synuclein and rotenone interaction, Biomolecules 3 (2013) 703–732.
[78] A. Rekas, R.B. Knott, A. Sokolova, K.J. Barnham, K.A. Perez, C.L. Masters, S. C. Drew, R. Cappai, C.C. Curtain, C.L.L. Pham, The structure of dopamine induced α-synuclein oligomers, Eur. Biophys. J. 39 (2010) 1407–1419.
[79] X.-J. Lin, F. Zhang, Y.-Y. Xie, W.-J. Bao, J.-H. He, H.-Y. Hu, Secondary structural formation of α-synuclein amyloids as revealed byg-factor of solid-state circular dichroism, Biopolymers 83 (2006) 226–232.
[80] J. Burré, S. Vivona, J. Diao, M. Sharma, A.T. Brunger, T.C. Südhof, Properties of native brain α-synuclein, Nature 498 (2013) 107–110.
[81] N.P. Ulrih, C.H. Barry, A.L. Fink, Impact of Tyr to ala mutations on α-synuclein fibrillation and structural properties, Biochim. Biophys. Acta Mol. basis Dis. 1782 (2008) 581–585.
[82] M.M. Apetri, N.C. Maiti, M.G. Zagorski, P.R. Carey, V.E. Anderson, Secondary structure of α-synuclein oligomers: characterization by Raman and atomic force microscopy, J. Mol. Biol. 355 (2006) 63–71.
[83] N.C. Maiti, M.M. Apetri, M.G. Zagorski, P.R. Carey, V.E. Anderson, Raman spectroscopic characterization of secondary structure in natively unfolded proteins: α-synuclein, J. Am. Chem. Soc. 126 (2004) 2399–2408.
[84] W. Bermel, I. Bertini, I.C. Felli, Y.M. Lee, C. Luchinat, R. Pierattelli, Protonless NMR experiments for sequence-specific assignment of backbone nuclei in unfolded proteins, J. Am. Chem. Soc. 128 (2006) 3918–3919.
[85] T. Kowalik-Jankowska, A. Rajewska, E. Jankowska, Z. Grzonka, Copper(ii) binding by fragments of α-synuclein containing M 1-D2- and -H50-residues; a combined potentiometric and spectroscopic study, *Dalt*, Trans. (2006) 5068–5076.
[86] M.D. Tuttle, G. Comellas, A.J. Nieuwkoop, D.J. Covell, D.A. Berthold, K. D. Kloepper, J.M. Courtney, J.K. Kim, A.M. Barclay, A. Kendall, W. Wan, G. Stubbs, C.D. Schwieters, V.M.Y. Lee, J.M. George, C.M. Rienstra, Solid-state NMR structure of a pathogenic fibril of full-length human α-synuclein, Nat. Struct. Mol. Biol. 23 (2016) 409–415.
[87] D.E. Mor, S.E. Ugras, M.J. Daniels, H. Ischiropoulos, Dynamic structural flexibility of α-synuclein, Neurobiol. Dis. 88 (2016) 66–74.
[88] L. Xu, R. Nussinov, B. Ma, Coupling of the non-amyloid-component (NAC) domain and the KTK(E/Q)GV repeats stabilize the α-synuclein fibrils, Eur. J. Med. Chem. 121 (2016) 841–850.
[89] H. Yu, W. Han, W. Ma, K. Schulten, Transient β -hairpin formation in α -synuclein monomer revealed by coarse-grained molecular dynamics simulation, J. Chem. Phys. 143 (2015), 243142.
[90] J. Gallardo, C. Escalona-Noguero, B. Sot, Role of α-synuclein regions in nucleation and elongation of amyloid fiber assembly, ACS Chem. Neurosci. 11 (2020) 872–879.
[91] F.A. Buratti, N. Boeffinger, H.A. Garro, J.S. Flores, F.J. Hita, P. do C. Gonçalves, F. D.R. Copello, L. Lizarraga, G. Rossetti, P. Carloni, M. Zweckstetter, T.F. Outeiro, S. Eimer, C. Griesinger, C.O. Fernández, Aromaticity at position 39 in α-synuclein: a modulator of amyloid fibril assembly and membrane-bound conformations, Protein Sci. 31 (2022), e4360.
[92] R. Moons, A. Konijnenberg, C. Mensch, R. Van Elzen, C. Johannessen, S. Maudsley, A.M. Lambeir, F. Sobott, Metal ions shape α-synuclein, Sci. Rep. 10 (2020) 1–13.
[93] H.T. Li, H.N. Du, L. Tang, J. Hu, H.Y. Hu, Structural transformation and aggregation of human α-synuclein in trifluoroethanol: non-amyloid component sequence is essential and β-sheet formation is prerequisite to aggregation, Biopolymers 64 (2002) 221–226.

[94] H. Wang, C. Mörman, R. Sternke-Hoffmann, C.-Y. Huang, A. Prota, P. Ma, J. Luo, Cu2+ ions modulate the interaction between α-synuclein and lipid membranes, J. Inorg. Biochem. 236 (2022), 111945.
[95] A.S. Maltsev, J. Chen, R.L. Levine, A. Bax, Site-specific interaction between α-synuclein and membranes probed by NMR-observed methionine oxidation rates, J. Am. Chem. Soc. 135 (2013) 2943–2946.
[96] M.C. Miotto, E.E. Rodriguez, A.A. Valiente-Gabioud, V. Torres-Monserrat, A. Binolfi, L. Quintanar, M. Zweckstetter, C. Griesinger, C.O. Fernández, Site-specific copper-catalyzed oxidation of α-synuclein: tightening the link between metal binding and protein oxidative damage in Parkinson's disease, Inorg. Chem. 53 (2014) 4350–4358.
[97] I. Horvath, S. Blockhuys, D. Šulskis, S. Holgersson, R. Kumar, B.M. Burmann, P. Wittung-Stafshede, Interaction between copper chaperone Atox1 and Parkinson's disease protein α-synuclein includes metal-binding sites and occurs in living cells, ACS Chem. Neurosci. 10 (2019) 4659–4668.
[98] C.C. Jao, B.G. Hegde, J. Chenb, I.S. Haworth, R. Langen, Structure of membrane-bound α-synuclein from site-directed spin labeling and computational refinement, Proc. Natl. Acad. Sci. U. S. A. 105 (2008) 19666–19671.
[99] M. Runfola, A. De Simone, M. Vendruscolo, C.M. Dobson, G. Fusco, The N-terminal acetylation of α-synuclein changes the affinity for lipid membranes but not the structural properties of the bound state, Sci. Rep. 10 (2020) 1–10.
[100] A. Pineda, J. Burre, Modulating membrane binding of α-synuclein as a therapeutic strategy, Proc. Natl. Acad. Sci. U. S. A. 114 (2017) 1223–1225.
[101] H.J. Lee, C. Choi, S.J. Lee, Membrane-bound α-synuclein has a high aggregation propensity and the ability to seed the aggregation of the cytosolic form, J. Biol. Chem. 277 (2002) 671–678.
[102] I. Dikiy, D. Eliezer, N-terminal acetylation stabilizes N-terminal helicity in lipid- and micelle-bound α-synuclein and increases its affinity for physiological membranes, J. Biol. Chem. 289 (2014) 3652–3665.
[103] D. Eliezer, E. Kutluay, R. Bussell, G. Browne, Conformational properties of α-synuclein in its free and lipid-associated states, J. Mol. Biol. 307 (2001) 1061–1073.
[104] V.N. Uversky, E.M. Cooper, K.S. Bower, J. Li, A.L. Fink, Accelerated α-synuclein fibrillation in crowded milieu, FEBS Lett. 515 (2002) 99–103.
[105] S. Bhattacharya, L. Xu, D. Thompson, Molecular simulations reveal terminal group mediated stabilization of helical conformers in both amyloid-β42 and α-synuclein, ACS Chem. Neurosci. 10 (2019) 2830–2842.